Food Research International 193 (2024) 114808

Contents lists available at ScienceDirect

Food Research International

journal homepage: www.elsevier.com/locate/foodres

Multiscale modeling of solid starch-based foods digestion in the intestinal tract for dietary property-based glycemic prediction

Yifan Qin [a,b], Jie Xiao [b,*], Aibing Yu [a,c], Xiao Dong Chen [b,*]

[a] Department of Chemical Engineering and Biological Engineering, Monash University, Clayton, Vic 3800, Australia
[b] School of Chemical and Environmental Engineering, College of Chemistry, Chemical Engineering and Materials Science, Soochow University, Suzhou, Jiangsu Province 215123, China
[c] Southeast University-Monash University Joint Research Institute, Suzhou Industrial Park, Suzhou, Jiangsu Province 215123, China

ARTICLE INFO

Keywords:
Multiscale modeling
Intestinal digestion
Mass transfer
Starchy particle
Glycemic prediction
Bioavailability

ABSTRACT

The digestion of starch-based foods in the intestinal tract is important for human health. Modeling the details enhances fundamental understanding and glycemic prediction accuracy. It is, however, a challenge to take granular properties into account. A multiscale digestion model has been proposed to characterize mass transfer and hydrolysis reaction at both the intestine and particle scales, seamlessly integrating inter-scale mass exchange. A specific grid scheme was formulated for the shrinkage and transport of the particle computational domain. By incorporating additional glycemic-related processes, e.g., intestinal absorption, a dietary property-based glycemic prediction system has been developed. Its effectiveness was validated based on a human tolerance experiment of cooked rice particles. The model-based investigation comprehensively reveals the impact of initial size on digestion behavior, specifically in terms of enzyme distribution and particle evolution. This work also demonstrates the significance of modeling both particle-scale diffusion and intestine-scale transport, a combination not previously explored. The results indicate that ignoring the former mechanism leads to an overestimation of the glycemic peak by at least 50.8%, while ignoring the latter results in an underestimation of 16.3%.

1. Introduction

Starch, a vital component in cereals, is the primary source of energy in the human daily diet. The starch digestion results in the release of glucose into the gut and the blood. Researchers in the food industry generally modify or process starch-based foods with consideration to the glycemic index (GI), which indicates the ability of a food to raise the blood glucose level. Numerous experimental studies evidenced the close connection between glycemic index and dietary properties, e.g., enzyme susceptibility (Bajaj et al., 2018), granular architecture (Dhital et al., 2017), granular size (Mackie et al., 2017) and indigestible component (Nilsson et al., 2006).

Due to the high cost of human meal tolerance tests, most researchers in the area of food or nutrition are currently compelled to calculate the glycemic index by *in-vitro* digestion experiments combined with an empirical function (Goñi et al., 1997; Nadia et al., 2021). However, this method is limited in practice because of the difference between *in and vivo* and *in-vitro* digestive environment. The distribution of digestive enzymes in the intestinal tract, for instance, is temporal- and spatial-dependent owing to the continuous secretion mode and the slow transport in this slender tubular organ. In contrast, the enzyme concentration during an *in-vitro* trail is well-distributed in a very short time. It could give rise to a distinct digestion behavior. In addition, *in-vitro* experimental equipment excludes various *in-vivo* processes related to the blood glucose regulation, e.g., gastric emptying, intestinal absorption and insulin action, which could lead to increased errors in estimating the glycemic index. An alternative approach is the blood glucose prediction model, which involves all the glycemic related processes (Oviedo et al., 2017). However, existing models fail to account for the effects of dietary properties. This significant defect also stems from inadequate modeling of the digestion process in organs prior to the bloodstream. Notably, the primary site for starch digestion is the small intestine (Lentle and Janssen, 2011). Therefore, it is very crucial to develop an intestinal digestion model that takes both the intestinal environment and the food properties into account.

The 1D distributed parameter model capable of capturing spatial-dependent characteristics has been frequently applied to describe mass

* Corresponding authors.
E-mail addresses: jie.xiao@suda.edu.cn (J. Xiao), xdchen@mail.suda.edu.cn (X. Dong Chen).

https://doi.org/10.1016/j.foodres.2024.114808
Received 6 April 2024; Received in revised form 2 July 2024; Accepted 21 July 2024
Available online 26 July 2024

Nomenclature

A_i	Interfacial area per unit granular volume [m^2/m^3]
A_p	Available surface area of a particle [m^2]
$C_{l,x}$	Concentration of a component in the small intestine [kg/m^3]
$C_{p,x}$	Concentration of a component in the particle [kg/m^3]
d_{pore}	Pore diameter [m]
d_x	Hydrodynamic diameter of a component [m]
$D_{p,x}$	Diffusivity of a component in a porous particle [m^2/s]
f	Increase ratio of absorptive surface area due to microstructures [-]
J_e	Secretion rate of enzyme [U/s]
J_p	Gastric emptying rate of starch particles [kg/s]
k_a	Absorption coefficient of glucose in the small intestine [m/s]
k_B	Boltzmann constant [-]
k_m	Reaction kinetics coefficient of maltose hydrolysis [m/s]
K_m	Adsorption constant [U/m^3]
L	Length of the small intestine [m]
L_p	Length of a cylindrical particle [m]
M_0	Total mass of starch particles ingested [kg]
$M_{p,m}$	Mass of maltose in a particle [kg]
n_p	Number of particles per unit volume of the intestine [$1/m^3$]
n_{sto}	Number of particles in the stomach [-]
P	Ratio of digestion or absorption [%]
q_s	Rate of starch dissociated from the solid–liquid interfere [$kg/(m^3 \cdot s)$]
$Q_{p,rel}$	Rate of maltose released from a particle [kg/s]
$Q_{p,h}$	Total hydrolysis rate of a starch particle [kg/s]
$Q_{p,i}$	Rate of starch hydrolysis inside a particle [kg/s]
$Q_{p,s}$	Rate of starch hydrolysis on the surface of a particle [kg/s]
r	Radial distance to the core of a particle [m]
r^*	a new positional variable equal to r/R_p [-]
R_i	Radius of the small intestine [m]
R_p	Radius of the particle [m]
S_{sm}	Rate of maltose released from particles [$kg/(m^3 \cdot s)$]
S_{mg}	Hydrolysis rate of maltose [$kg/(m^3 \cdot s)$]
S_{abs}	Absorption rate of glucose [$kg/(m^3 \cdot s)$]
$S_{l,x}$	Sink term of the intestine-scale model [$kg/(m^3 \cdot s)$]
$S_{p,x}$	Sink term of the particle-scale model [$kg/(m^3 \cdot s)$]
t_{emp}	Time when a particle is emptied into the intestine [s]
t	Time [s]
T	Absolute temperature [K]
$\overline{u}$	Average flow velocity of chyme in the small intestine [m/s]
V_0	Initial volume of a particle [m^3]
V_{max}	Maximum rate of starch hydrolysis per unit area [$kg/(m^2 \cdot s)$]
X	Solid mass per unit particle volume [kg/m^3]
ΔG	Glycemic change [mmol/L]
ρ_0	Initial particle density [kg/m^3]
κ_{mg}	Mass increase ratio when converting maltose to glucose [-]
κ_{sm}	Mass increase ratio when converting starch to maltose [-]
λ	Parameter that determines the geometry of the particle [-]
η	Ratio of indigestible component [-]
ε	Porosity [-]
τ	Tortuosity factor [-]
μ	Viscosity [Pa·s]
ω	Digestion or absorption amount per unit intestinal length [kg/m]
γ	Rate constant of gastric emptying [s^{-1}]
Φ	Rate of digestion or absorption in small intestine [kg]

transfer and chemical reactions in a tubular intestinal tract, which was systematically reviewed by Qin et al. (2023a). However, the majority of previous efforts only focused on the intestinal absorption of nutrients or drugs. For a sake of adding the starch digestion, Moxon et al. (2016) applied the Michaelis-Menton function, which described the saturation effect of substrate on the enzymatic reaction. Although parameter values of this empirical function for various starches have been estimated through *in-vitro* digestion experiments, their accuracy for the *in-vivo* calculation is questionable. Furthermore, this function is sound for the digestion reaction in a homogenous system, e.g., aqueous solutions of gelatinized starch, but not feasible for that in a heterogeneous system, e.g., suspensions of granular starch. Solid starch-based foods like cereal grains are porous structures consisting of starch and other components, e.g., fibers. The hydrolysis rate depends not only on the enzyme sensitivity to substrate but also on granular architecture factors such as size and porosity. These properties can be altered through food processing or modification. Cooked rice, for example, typically exhibits a more open granular network and a more digestible crystalline structure of starch (Dhital et al., 2017). Recently, our team successfully developed a starch particle hydrolysis model capable of accounting for the effects of granular intrinsic properties (Qin et al., 2023b). It was proved effective in predicting the *in-vitro* digestive behaviors of both raw and cooked starch-based particles. For an *in-vivo* digestion scenario, the particle hydrolysis model should be coupled with the intestinal distributed parameter model.

It is a typically multiscale modeling problem. The boundary conditions of the microscale fields at the particle surface are provided by the solution of the macroscale model equations, while the mass source terms of the macroscale model equations are determined by the mass transferred from particles. Despite numerous successful cases in engineering fields, e.g., fixed-bed reactors (Park, 2018), modeling mass transfer and enzymatic reaction in an intestinal granular system remains a significant challenge. Firstly, unlike porous catalysts that have been extensively studied, cereal particles are reactants with natures (e.g., size, porosity, ratio of indigestible component, etc.) that change over time. Particularly, the reduction in particle size results in a shrinking computational domain of the particle model, increasing the complexity of numerical solving. Moreover, particles in an intestinal system, different from those in a fixed-bed reactor, flow forward together with the fluid. This means that the position of a particle, as well as the localized number of particles, are both temporal-dependent variables. The challenge is how to express mathematically the transport of the information at the particle scale along the intestine.

This work aims to develop a multiscale digestion model that comprehensively characterizes the transport and evolution of starch-based particles in the intestinal tract. The mass transfer of enzyme and hydrolysates at intestinal and granular scales as well as the inter-scale mass exchange will be modeled. An innovative grid scheme will be proposed to deal with the shrinking particle computational domain and its movement along the intestine. This paper will also incorporate other *in-vivo* processes related to the glycemic response, e.g., gastric emptying, maltose hydrolysis, glucose absorption and glucose-insulin interaction, to generate a dietary property-based glycemic prediction system. It will account for not only the enzyme sensitivity to substrate but also the granular properties, e.g., size, shape, porosity and pore size. This will be the first attempt to predict the effect of granular properties on the blood glucose response based on principles of mass transfer and chemical reaction. In addition, the significance of simultaneously modeling

diffusion resistance within the particle and transport phenomenon along the intestine for digestive prediction will be analyzed to prove the superiority of the multiscale modeling approach.

2. Model development

Fig. 1 illustrates the development of the *in-vivo* digestion model separately at two scales: the intestinal scale and the particle scale. The small intestine is analogous to a straight full flow pipe. Solid starch-based particles are assumed to be spheres composed of starch and indigestible components. Particles of uniform size are continuously emptied at the entrance, also called the pylorus. The digestive process in the stomach is ignored as the starch hydrolysis reaction is suppressed by gastric acid. The digestive enzyme, i.e., α-amylase, is secreted at the starting point of the lumen. When moving forward along the tract together with particles, the enzyme in the fluid gradually permeates inward the particle interior, and catalyzes the starch hydrolysis. As drawn in the particle-scale view of Fig. 1, both the changes in particle size and internal structure are captured in this model. The hydrolysis product is exclusively assumed to be maltose in that oligosaccharides are too various. After escaping from the particle into the bulk space, maltose is converted further to glucose by the action of brush border enzyme on the inner surface of the intestinal wall. Then glucose is absorbed by epithelial cell into the blood where it will be regulated by the action of insulin.

2.1. Intestine-scale model

The substrate transport, chemical reaction and nutrient absorption in the intestinal tract can be described mathematically by a 1D advection-reaction equation, which has been widely applied by previous studies (Qin et al., 2023a).

$$\frac{\partial C_{l,x}}{\partial t} = -\bar{u}\frac{\partial C_{l,x}}{\partial z} + S_{l,x}$$

$$C_{l,x}\big|_{z=0} = C_{x,0}$$

$$C_{l,x}\big|_{t=0} = 0 \tag{1}$$

Here $C_{l,x}$ denotes the concentration of species x at time t and distance from the pylorus z. Species in the fluid involve enzyme ($x = e$), maltose ($x = m$) and glucose ($x = g$). While the units for the latter two components are both kg/m^3, the unit for enzyme is expressed as U/m^3. U is an international unit of enzyme catalytic activity, and 1 U is defined as the amount of enzyme that catalyzes the conversion of 1 μmol of substrate per minute. Under the premise of constant temperature and pH, the ability to convert the substrate is directly proportional to the enzyme amount (van Boekel, 2008). U/m^3 can thus be regarded as a concentration unit. The model describes a one-dimensional process of perfect mixing at each cross-section, which is a general assumption for 1D intestinal modeling (Qin et al., 2023a). $\bar{u}$ [m/s] is the average velocity of the solid–liquid mixture as it moves along the axial direction. As a first approximation, it is assumed that particles are transported along with the fluid at the same velocity. The spatial distribution of particles can be expressed in a similar form:

$$\frac{\partial n_p}{\partial t} = -\bar{u}\frac{\partial n_p}{\partial z}$$

$$n_p\big|_{z=0} = n_{p,0}$$

$$n_p\big|_{t=0} = 0 \tag{2}$$

where n_p [1/m^3] is the localized number of particles per unit volume of the intestine.

The Dirichlet boundary condition imposed on Eq. (1) specifies the concentration at the inlet. The inlet concentrations of the hydrolysis products, maltose and glucose, are both zero. The value for α-amylase, which catalyzes the first step of the starch digestion, is dependent on the secretion rate from the pancreas. Given that the pancreatic secretion port is located very close to the pylorus (less than 10 cm), a distance that is negligible compared to the total length of the gut (Guyton and Hall, 2006), the enzyme is approximated to be injected at the intestinal entrance. Many experimental investigators have observed a marked but short increase in the pancreatic α-amylase output followed by a fast decline after the ingestion of carbohydrate-rich meals (Keller and Layer, 2005). Based on this observation, we propose an empirical function that controls the secretion rate J_e [U/s]. The data reported by Czakó et al. (1999) is referred for parameter fitting.

$$J_e = \frac{a}{t^b + \frac{c}{t+d}} + h \tag{3}$$

where a = 4.93 × 10^6, b = 1.88, c = 2.74 × 10^8, d = 294, h = 5.82. The regression curve, along with the original data, is displayed in Fig. 2. The goodness of fit is evaluated as 0.9773.

The boundary concentration of enzyme is then determined by the

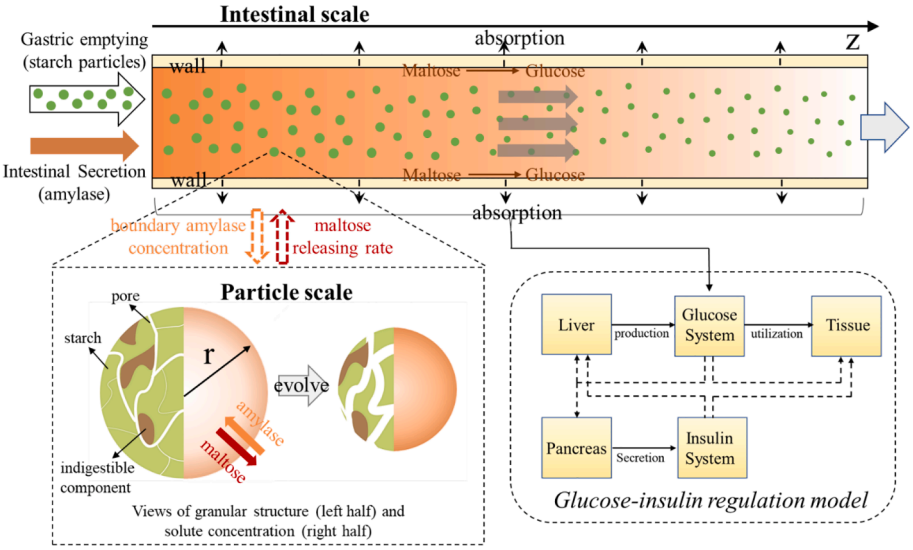

Fig. 1. Multiscale illustration of starch-based particle digestion in the small intestine as well as maltose reaction, glucose absorption and insulin regulation.

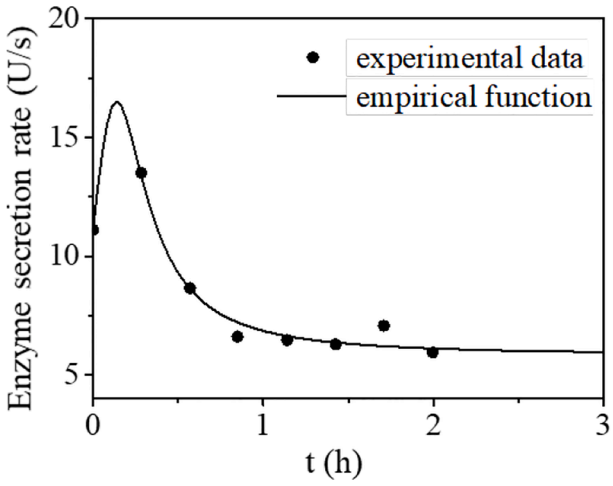

Fig. 2. Pancreatic α-amylase secretion in response to carbohydrate meal (Czakó et al., 1999).

following equation:

$$C_{l,e}\big|_{z=0} = \frac{J_e}{\pi R_i^2 \overline{u}} \tag{4}$$

Here R_i [m] represents the radius of the small intestine.

The boundary condition for Eq. (2) can be expressed as:

$$n_{p,0} = \frac{J_p}{\pi R_i^2 \overline{u}} \tag{5}$$

Here J_p [kg/s] denotes the gastric emptying rate of particles, which adheres to first-order kinetics (Moxon et al., 2016):

$$J_p = \gamma n_{sto} = -\frac{\partial n_{sto}}{\partial t}$$

$$n_{sto}\big|_{t=0} = \frac{M_0}{\rho_0 V_0} \tag{6}$$

where n_{sto} represents the number of particles in the stomach. Its initial value is calculated by the total mass of ingested particles M_0, the initial granular density ρ_0, and the initial volume of a particle V_0. γ [1/s] is the rate constant of gastric emptying which is computed by the empirical function proposed by Dalla Man et al. (2006).

In Eq. (1), $S_{l,x}$ is the sink term that represents the reaction rate or absorption rate. For enzyme, it is zero since enzyme is not consumed or absorbed. For maltose, it is composed of a positive mass source released from particles S_{sm} [kg/(m^3·s)] and a negative mass consumption due to the hydrolysis of maltose S_{mg} [kg/(m^3·s)]. For glucose, it consists of the production rate $\kappa_{mg}S_{mg}$ [kg/(m^3·s)] and the absorption rate of glucose S_{abs} [kg/(m^3·s)].

$$S_{l,x} = \begin{cases} 0 & \mathrm{x = enzyme} \\ S_{sm} - S_{mg} & \mathrm{x = maltose} \\ \kappa_{mg}S_{mg} - S_{\mathrm{abs}} & \mathrm{x = glucose} \end{cases} \tag{7}$$

where κ_{mg} is the mass increase ratio when converting maltose to glucose (162:171). Both the reaction of maltose and the absorption of glucose are processes that occur on the inner surface of the intestinal lumen. Their rates can be expressed using the following formulas, respectively.

$$S_{mg} = \frac{2fk_m}{R_i} C_{l,m} \tag{8}$$

$$S_{abs} = \frac{2fk_a}{R_i} C_{l,g} \tag{9}$$

where f is the increase ratio of absorptive surface area due to microstructures on the inner wall, e.g., fold, villi, microvilli. k_m [m/s] is the reaction kinetics coefficient of maltose hydrolysis. k_a [m/s] is the absorption coefficient of glucose in the small intestine.

2.2. Particle-scale model

This section delves into the intricacies of mass transfer and enzymatic reaction at the particle level. In the prior work, we successfully established a diffusion–reaction model that effectively characterizes hindered enzyme diffusion and substrate hydrolysis within porous starch particles (Qin et al., 2023b). However, it was specifically designed for *in-vitro* digestion experiments, assuming constant external conditions surrounding the particle. Notably, *in-vivo* digestion systems present a dynamic environment where the external conditions of a particle vary both temporally and spatially. The primary contribution herein is the improvement of the model to accurately adapt the dynamic *in-vivo* environment.

The general form of the equation describing solute diffusion and enzymatic reaction within a particle is written as follows:

$$\begin{aligned} &\frac{\partial C_{p,x}}{\partial t} = \frac{1}{r^{\lambda-1}} \frac{\partial}{\partial r}\left(D_{p,x} r^{\lambda-1} \frac{\partial C_{p,x}}{\partial r}\right) + S_{p,x} \\ &\frac{\partial C_{p,x}}{\partial r}\bigg|_{r=0} = 0 \\ &C_{p,x}\big|_{r=R_p} = C^s_{p,x} \end{aligned} \tag{10}$$

Here $C_{p,x}$ denotes the concentration of enzyme [U/m^3] or maltose [kg/m^3] at a distance r from the core of a particle. The superscript λ (equal to 2 or 3) indicates the particle shape (cylinder or sphere). $C^s_{p,x}$ is the concentration on the particle surface. $D_{p,x}$ [m^2/s] refers to the diffusivity of a component in a porous particle. It is related to several granular properties, e.g., porosity, tortuosity, pore diameter, solvent viscosity and the diffusing solute.

The sink term in Eq. (10), which varies for different components, is expressed as follow:

$$S_{p,x} = \begin{cases} 0 & x = enzyme \\ \kappa_{sm} q & x = maltose \end{cases} \tag{11}$$

The former clarifies that the enzyme is neither consumed nor produced during the hydrolysis process. The latter specifies the rate of maltose production. The coefficient κ_{sm} is the mass increase ratio when starch is converted to maltose (162:171). q [kg/(m^3·s)] denotes the rate at which starch dissociates from the solid–liquid interface.

$$q = -\frac{\partial X_{dig}}{\partial t} = \frac{V_{max} A_i (1-\eta) C_{p,e}}{K_m + C_{p,e}} \tag{12}$$

Here X_{dig} [kg/m^3] is the mass of digestible starch per unit particle volume. V_{max} [kg/(m^2·s)], K_m [U/m^3], A_i [m^2/m^3] and η [-] are the maximum rate of starch hydrolysis per unit interfacial area, the adsorption constant, the interfacial area per unit granular volume and the ratio of indigestible component, respectively.

The rate of starch hydrolysis occurring inside a particle is determined by the following integral formula:

$$Q_{p,i} = \begin{cases} \int_0^{R_p} 2\pi r L_p q dr\lambda = 2 \\ \int_0^{R_p} 4\pi r^2 q dr\lambda = 3 \end{cases} \tag{13}$$

In addition to the interior space, the exterior surface of a particle also offers a large number of reactive sites. The rate of starch hydrolysis on the surface of a particle is given by the following expression

$$Q_{p,s} = \frac{V_{max} A_p (1-\eta_s) C_{l,e}}{K_m + C_{l,e}} \tag{14}$$

The available surface area A_p [m^2] is influenced by the granular geometry λ, the size R_p and the porosity on the surface ε_s. For a cylinder, the formula accounts for the surface area excluding the two ends as the diffusion–reaction equation Eq. (10) fails to consider diffusion and reaction along the axial direction of the cylinder.

$$A_p = \begin{cases} 2\pi R_p L_p (1-\varepsilon_s)\lambda = 2 \\ 4\pi {R_p}^2 (1-\varepsilon_s)\lambda = 3 \end{cases} \tag{15}$$

The superficial dissociation of the particle inversely leads to a decrease in its size. When the digestible component on the surface is depleted, the particle ceases to shrink. The evolution of particle size can be expressed as:

$$\frac{dR_p}{dt} = \begin{cases} \dfrac{V_{max} C^s_{p,x} (1-\varepsilon_0)}{(K_m + C^s_{p,x})\rho_0} X^s_{dig} > 0 \\ 0 X^s_{dig} = 0 \end{cases} \tag{16}$$

The total hydrolysis rate of starch in a particle is the sum of Eq. (13) & (14):

$$Q_{p,h} = Q_{p,i} + Q_{p,s} \tag{17}$$

The mass of maltose within a particle can be calculated by integrating the local concentration over the particle volume:

$$M_{p,m} = \begin{cases} \int_0^{R_p} 2\pi r L_p C_{p,m} dr\lambda = 2 \\ \int_0^{R_p} 4\pi r^2 C_{p,m} dr\lambda = 3 \end{cases} \tag{18}$$

The mass balance principle stipulates that the rate of maltose released from a particle equals the rate of its production minus the rate of change of its mass:

$$Q_{p,rel} = \kappa_{sm} Q_{p,h} - \frac{\partial M_{p,m}}{\partial t} \tag{19}$$

Formulas for the remaining variables are listed in Appendix A without detailed explanations as they remain unchanged compared with the original version (Qin et al., 2023b).

2.3. Multiscale coupling

The bidirectional coupling between the macroscopic and microscopic models, depicted in Fig. 1, is straightforward. The sets of equations for different scales can obtain the distributions of a specific component in the intestine and within the particle at any given time, respectively. Identifying the real-time position of a particle in the intestinal tract is essential, enabling the access of the corresponding boundary conditions from the intestinal model and the export of mass sources from particles at their corresponding positions. To achieve it, a new independent variable is introduced, specifically the time when a particle is emptied into the intestine t_{emp},

$$z = (t - t_{emp})\overline{u} \tag{20}$$

Here $t - t_{emp}$ represents the time a particle takes to travel from the pylorus. This equation defines the forward transport of the particle-scale information:

$$C_{p,x}(r, z, t) = C_{p,x}(r, t_{emp}, t) \tag{21}$$

On this basis, the concentration fields in the intestinal tract align with the boundary conditions of particles injected at different times. Given the assumption of the perfect mixing over the cross section of the intestine, the concentration of enzyme or maltose on the particle surface can be regarded equivalent to the bulk concentration at the particle's current position.

$$C^s_{p,x}(t_{emp}, t) = C_{l,x}(z, t) \tag{22}$$

Regarding the positive mass source of maltose released from particles into the fluid (see Eq. (7)), it can be calculated based on the localized particle number n_p and the releasing rate of maltose from the corresponding particle $Q_{p,rel}$:

$$S_{sm}(z, t) = n_p(z, t) Q_{p,rel}(t_{emp}, t) \tag{23}$$

2.4. Quantification method

The developed model is capable of comprehensively capturing the behaviors of digestion and absorption in the intestinal tract. The rates [kg/s] of starch digestion and glucose absorption can be calculated by Eq. (24)–(25).

$$\Phi_{dig}(t) = \int_0^L \pi {R_i}^2 n_p Q_{p,h} dz \tag{24}$$

$$\Phi_{abs}(t) = \int_0^L \pi {R_i}^2 G_{abs} dz \tag{25}$$

where L [m] and R_i [m] are length and radius of the small intestine, respectively. The proportions of starch digestion and glucose absorption over time are thus quantified as:

$$P_{dig}(t) = \frac{\int_0^t \Phi_{dig} dt}{M_0(1-\eta_0)} \times 100\% \tag{26}$$

$$P_{abs}(t) = \frac{\int_0^t \Phi_{abs} dt}{M_0(1-\eta_0)\kappa_{sg}} \times 100\% \tag{27}$$

To assess the performances of digestion and absorption in different segments of the intestine, the amounts per unit intestinal length over a specific period can be computed by the following equations.

$$\omega_{dig}(z) = \int_0^T \pi {R_i}^2 n_p Q_h dt \tag{28}$$

$$\omega_{abs}(z) = \int_0^T \pi {R_i}^2 G_{abs}(C_{l,g}) dt \tag{29}$$

Moreover, numerical experiments conducted by this model enable the observation of changes in food properties as it progresses through the intestine. One key aspect is the degree of decrease in starch proportion, characterized by the ratio $\overline{X}_{dig}/X_{dig,0}$. The average mass of starch per unit granular volume $\overline{X}_{dig}$ [kg/m^3] can be calculated based on its spatial distribution within a particle

$$\overline{X}_{dig} = \frac{3\int_0^{R_p} r^2 X_{dig} dr}{R_p^3} \tag{30}$$

In this transient system, the distributions of particles and enzyme are nonuniform, with concentrations even dropping to zero in the posterior segment of the intestinal tract. Consequently, the average concentration over the whole intestine is unable to accurately represent the concentration level surrounding particles. To better evaluate the intestinal environment for particles digestion, the average concentration of enzyme surrounding all particles is defined:

$$\overline{C^s_{p,e}} = \frac{\int_0^L C_{l,e} n_p dz}{\int_0^L n_p dz} \tag{31}$$

An established glycemic prediction model, which has been recognized by FDA as a substitute to animal testing for preclinical trials of closed-loop control strategies, is applied to generate glycemic data. It is achieved by using the glucose absorption rate Φ_{abs} from the newly proposed digestion model as a time series input of the glucose-insulin

regulation system, whose equations and parameter values were listed in detail by Dalla Man et al. (2007). The glycemic change ΔG is calculated by subtracting fasting value from real-time value.

The coefficient of determination R^2 is used to evaluate the predictive accuracy of the developed model:

$$R^2 = 1 - \frac{\sum_{n=1}^{N}\left(y_{exp}^{n} - y_{sim}^{n}\right)^2}{\sum_{n=1}^{N}\left(y_{exp}^{n} - \overline{y_{exp}}\right)^2} \tag{32}$$

where N denotes the number of the sampling points in an experiment. y_{exp}^{n} is the n-th experimental data, and y_{sim}^{n} is the simulation data at the same sampling time. $\overline{y_{exp}}$ is the average value of all experimental data. This indicator goes below 1, where 1 indicates a perfect model performance.

2.5. Numerical method

The numerical solving of the multiscale system is carried out by a finite difference method. Fig. 3. Illustrates the discretization schemes employed for the computational domain at different scales. A matrix of dimensions (kmax, imax) is inverted at each time step. Here, *kmax* is the grid number for the particle-scale coordinate and *imax* is the grid number for the intestine-scale coordinate. The convection-reaction equations at the intestinal scale, i.e., Eq. (1) & (2), are discretized by employing the upwind differencing method for the intestinal spatial domain and the forward Euler method for the temporal domain. In Fig. 3, the horizontal axis represents the grid division along the axial direction of the intestine, while the vertical axis illustrates the time stepping scheme. The time step is defined as Δt. To ensure the node-to-node mass exchange between the fluid and particles in a flow system, the grid size is determined based on a relationship derived from Eq. (20), that is $\Delta z = \overline{u}\Delta t$. It adheres to the stability condition for solving partial differential equations (PDE) using finite difference method according to the Von Neumann Analysis (Moxon et al., 2017).

The particle-scale diffusion–reaction equation, i.e., Eq (10), is discretized by using the centered difference scheme for the granular spatial domain and the forward Euler method for the temporal domain. The concentric circles denote the grid division along the radial direction of the particle. Particle shrinking over time is responsible for the evolution in the space discretization. A moving boundary method (Illingworth and Golosnoy, 2005) is applied to deal with the motion of the particle surface. A new positional variable $r^* = r/R_p$ is introduced to amend the physical domain $0 \le r \le R_p$ to the computational domain $0 \le r^* \le 1$. The spatial step is transformed to Δr^*. The modified form of Eq. (10) is thus given as follow:

$$\frac{\partial C_{p,x}}{\partial t} - \frac{r^*}{R_p}\frac{dR_p}{dt}\frac{\partial C_{p,x}}{\partial r^*} = \frac{1}{(r^*)^{\lambda-1}R_p{}^2}\frac{\partial}{\partial r^*}\left(D_{p,x}(r^*)^{\lambda-1}\frac{\partial C_{p,x}}{\partial r^*}\right) + S_{p,x} \tag{33}$$

The discretized forms are given in detail in Appendix B.

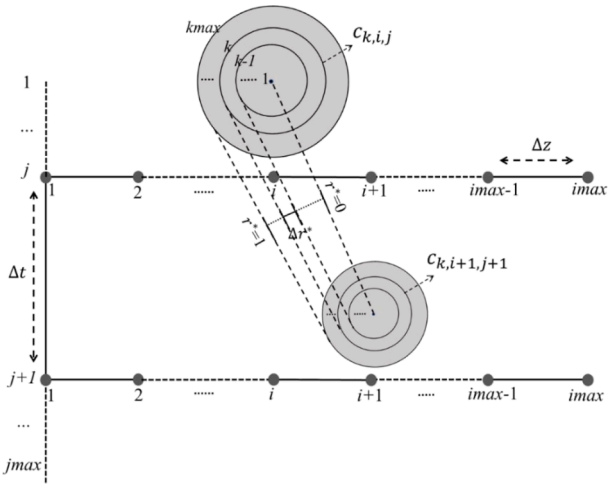

Fig. 3. Grid system for the multiscale model.

3. Results & discussion

3.1. Model validation

The efficacy of the developed model is evaluated based on previous human meal tolerance tests, of which the dietary conditions are listed in Table 1. In the experiment conducted by Ranawana et al. (2011), i.e., Group I and II, healthy volunteers consumed cooked rice differing in particle size and shape, and were instructed to swallow the food without chewing to ensure no change in particle size in the mouth. In the experiment conducted by Ranawana et al. (2010), i.e., Group III, the percentages of rice particles in different size categories after oral mastication were available. The average particle size for each category was estimated and used as the model input. The postprandial blood glucose data recorded in the two experiments is plotted in Fig. 4(b). Table 1 also provides the values of other parameters estimated by Qin et al. (2023b) for cooked rice particles. The physiological parameters and physiochemical properties obtained from published literature are given in Table 2.

Fig. 4(a) illustrate the results of starch digestion and glucose absorption, predicted based on dietary conditions of different references. In the initial period, the slopes of curves see a noticeable upward trend. It indicates an acceleration in the digestion rate as increasingly more substrate is emptied into the intestine and the enzyme progressively permeates into the interior of particles. It is clear that, for Group II, starch in particles is hydrolyzed at a higher rate. The same goes for the absorption rate. When the digestion percentage for Group I reaches about 60 % at 2 h, the particles in Group II are almost completely consumed. Group III, which exhibits a wide distribution of particle sizes, presents two stages of digestion. The dramatic climb in the early stage is driven by the rapid hydrolysis of small particles, whereas the sluggish increase in the later stage results from the inhibited reaction in large particles.

The changes in blood glucose levels were computed by the blood glucose-insulin interaction model using the absorption data in Fig. 4(a) as time-sequence input. Comparing Group I and Group II in Fig. 4(b), it is

Table 1
Properties of the ingested food in human meal tolerance experiments.

Reference	Ranawana et al., 2011		Ranawana et al., 2010
Group	I	II	III
Ingested food	Cooked Rice		
Total mass	64.8 g		
Starch ratio	0.776		
Shape	cylinder	sphere	sphere
Size	Length L_p: 11868 μm Diameter d_p: 1653 μm	Diameter d_p: 750 μm	Diameter d_p: 2000 μm (17 %) 1500 μm (7.5 %) 750 μm (2.4 %) 500 μm (73.1 %)
Maximum hydrolysis rate per unit area V_{max}	1.32×10^{-5} [kg/(m^2·s)] *		
Equilibrium constant K_m	1.1 [U/ml] *		
Porosity ε_0	0.48 *		
Available area per unit particle volume A_i	1.39×10^{5} [m^2/m^3] *		
Pore diameter d_{pore}	13.7 [nm] *		

*Values estimated by Qin et al. 2023(b) for cooked rice particles.

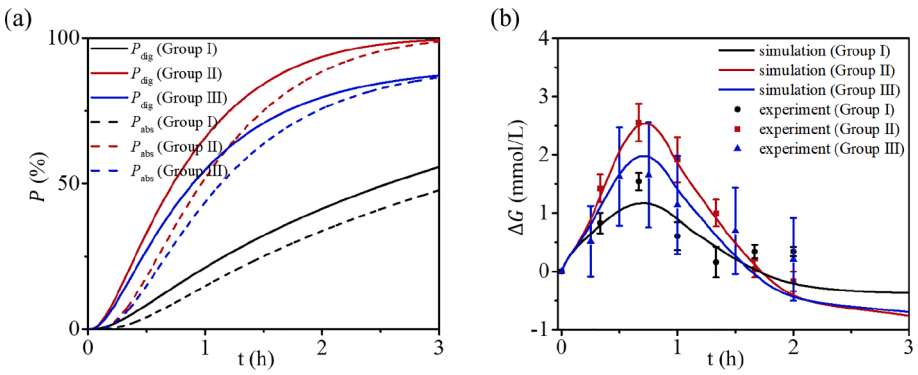

Fig. 4. Simulation results of Group I, II and III based on dietary conditions given in Table 1. (a) percentages of starch digestion and glucose absorption, and (b) glycemic change. Dots: experimental data of Groups I and II (Ranawana et al. 2011) and Group III (Ranawana et al., 2010).

Table 2
Values of physiological parameters used in the simulation.

Parameter	Value	Reference
Body mass	75 kg	(Ranawana et al., 2010; Ranawana et al., 2011)
Mean axial velocity $\overline{u}$	1.7×10^{-4} m/s	(Guyton and Hall, 2006)
Viscosity of chyme μ	0.01 Pa s	(Ellis et al., 1995)
Length of the small intestine L	3 m	(Tortora and Derrickson, 2018)
Diameter of small intestine R_i	1.25 cm	(Tortora and Derrickson, 2018)
Reaction coefficient of maltose k_m	1.5×10^{-6} m/s	(Dahlqvist and Thomson, 1963)
Absorption coefficient of glucose k_a	9.2×10^{-7} m/s	(Lennernäs et al., 1996)
Increase in absorption area due to microstructures f	12	(Moxon et al., 2016)
Diameter of α-amylase d_e	7 nm	(Payan et al., 1980)
Diameter of maltose d_m	1 nm	(Gres and Jeffrey, 1977)

evident that the simulated tendency of lowering glycemic concentration by increasing particle size is basically consistent with the clinic observation, characterized by a declining peak value, a constant peak time and a higher level in the later stage. The model shows superior predictive performance for Group II ($R^2 = 0.9886$) compared to Group I (R^2=0.5861). It may result from the physical breakdown in the stomach (Nadia et al., 2021), a factor not accounted for in this model. Large particles in Group I are likely to experience disruption to a higher extent during the gastric phase, leading to smaller particle size when the chyme enters the intestine. For the second experiment (i.e., Group III), the predicted glycemic change falls basically within the range of experimental error. Its value of R^2 (0.3224) is not high but acceptable for a complex human system. Comparing the two groups with spherical particles, it can be found that the predicted glycemic level of Group III is lower than that of Group II since the former contains a certain proportion of large particles.

3.2. *Effect of particle size on digestive behavior*

Four groups of rice particles differing in initial size (0.5 mm, 1 mm, 1.5 mm and 2 mm) are investigated in this section. The ingested mass in each group is 64.8 g, and the particle shape is controlled to be spherical. Fig. 5(a) plots the proportions of starch digestion and glucose absorption over time, while Fig. 5(b) displays the corresponding glycemic responses. They suggest that a reduction in particle size dramatically promotes the digestion rate, responsible for a lower glucose absorption rate and a sharper climb in blood glucose levels. Notably, the peak of glycemic change nearly triples when comparing initial particle size of 0.5 mm to 2 mm. This result can be further elucidated by Fig. 6, which depicts the concentration distributions of enzyme and maltose within particles along the intestine at different times. As the chyme progresses towards the end of the intestine, enzyme gradually diffuses into the granular interior. Smaller initial size is more conductive to enzyme penetration and maltose production in the particle core. Additionally, one can see higher enzyme concentration, either inside or outside the particles, at the head of chyme owing to the massive secretion of pancreatic enzyme at the early stage (see Fig. 2). It leads to faster starch hydrolysis, and consequently higher maltose concentration in this region.

It can also be found in Fig. 5(a) that, at three hours, the average gap between adjacent digestion curves (10.92 %) is narrower than that between adjacent absorption curves (14.01 %). It implies that initial particle diameter has a more pronounced impact on the proportion of glucose absorption in that the diffusion resistance of maltose within a particle makes an effect as well. As illustrated by the lower subgraphs in Fig. 6, maltose is initially produced in the outer region of a particle,

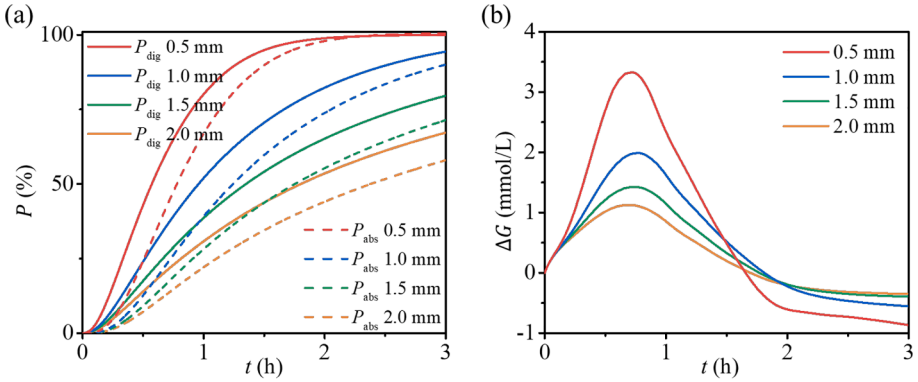

Fig. 5. Effect of initial particle size on (a) percentages of starch digestion and glucose absorption, and (b) glycemic change.

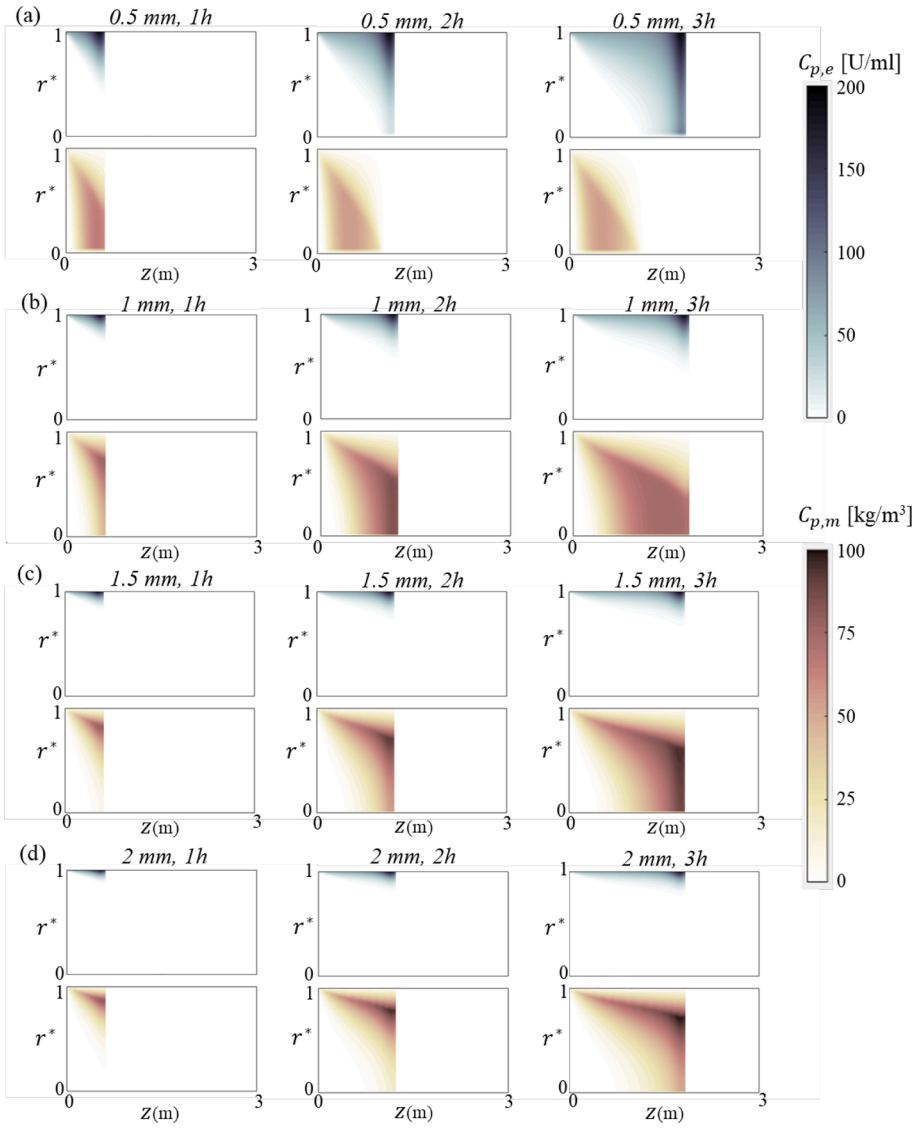

Fig. 6. Spatial profiles of enzyme concentration and maltose concentration along the radial direction of the particle and the axial direction of the intestine for different initial particle sizes (a) 0.5 mm, (b) 1 mm, (c) 1.5 mm and (d) 2 mm.

resulting in a decreasing profile of the maltose concentration from the outside in. Over time, the location of the maximum concentration shifts inward as maltose escapes. The surrounding concentration of maltose, equal to the concentration on the particle surface (see Eq. (22)), is extremely low throughout, maintaining a continuous concentration difference for outward mass transfer.

Computational experiments have an ability of revealing the detailed granular information during digestion. Fig. 7(a)&(b) display the spatial profiles of starch proportion in the particles and particle size along the intestinal tract. The curves at different times differ slightly due to the non-steady secretion of the enzyme, as depicted in Fig. 2. Finer grains experience a more dramatic change in both aspects. It is intriguing that, in Fig. 7(b), the particle shrinkage for all groups ceases at around 40 cm from the entrance as the digestible starch on the particle surface becomes depleted. However, the hydrolysis reaction in the granular interior in Fig. 7(a) is sustainable, allowing the majority of starch to be consumed in the intestinal tract. Such a high starch digestibility aligns with the measurement from a human experiment involving various starchy foods (Zhou et al., 2010). Fig. 7(c) indicates that the rates of both digestion and absorption per unit intestinal length are relatively higher in the duodenum, i.e., the first approximately 25 cm of the intestine. A previous experimental study also found a similar pattern of glycose absorption in the mouse intestine (Fatima et al., 2009).

The increase in food size delays the behaviors of digestion and absorption to a more distal segment. When comparing the digestion proportions among different intestinal segments, it is observed that more starch in particles larger than 0.5 mm is digested after the duodenum. It can be inferred that, foods more resistant to hydrolysis than rice would have a lower proportion of digestion occurring in the duodenum.

3.3. Significance of diffusion resistance within a particle

This section assesses the importance of modeling the diffusion process within the particle, which was previously overlooked in intestinal digestion modeling. A contrast model disregarding this step is introduced, defining that the enzyme concentration within the whole particle is equal to its surrounding concentration. In this model, the diffusion equation for enzyme, i.e., Eq. (10), is modified to:

$$C_{p,e} = C_{l,e} \tag{34}$$

Meanwhile, the generated maltose is instantaneously released into the surrounding space, bypassing diffusion process. It means that the rate of maltose released from a particle equals to its produced rate. Consequently, Eq. (20) is revised to the following equation:

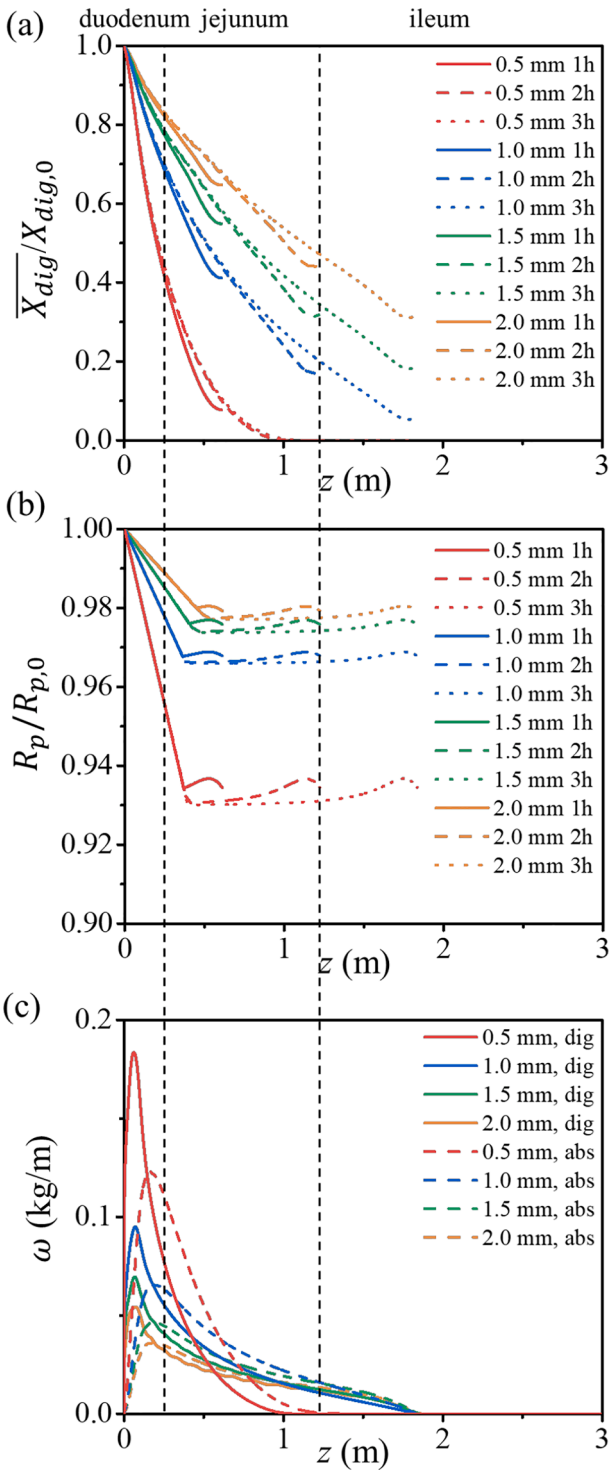

Fig. 7. Effect of initial particle size on (a) the evolution of the average proportion of digestible starch in the particle, (b) the evolution of particle radius, and (c) the amount of digestion and absorption per unit intestinal length over three hours.

$$Q_{p,rel} = \kappa_{sm} Q_{p,h} \tag{35}$$

The same four groups of rice particles differing in initial size (0.5 mm, 1 mm, 1.5 mm and 2 mm) are simulated by the contrast model. Their results, depicted by dashed lines in Fig. 8, demonstrate nearly identical levels. It indicates that the model without diffusion resistance fails to account for the effect of particle size. Comparing Fig. 8(a, b, c & d) in sequence, one can see increasingly more significant errors caused by ignoring the diffusion within particles as the initial particle size increases. From 0.5 mm to 2 mm, the gap in the digestion proportion at 1 h between the two models widens from 15.3 % to 64.6 %. Consequently, the predictive error in the maximum blood glucose concentration climbs from 50.8 % to 345.3 %. Meanwhile, the time to peak for all groups is undervalued by approximately 15 min as well.

The diffusion resistance might be rate-determining for starch digestion and glucose absorption when the initial size exceeds a certain value. Given that the rice particles researched in this work are characterized by rich pores, we can infer that this finding might be even more applicable to cereal grains lacking pores and channels, e.g., potato grain (Dhital et al., 2017). Lower porosity undoubtedly results in stronger mass transfer resistance. On the other hand, it also implies that the diffusion process within the particle smaller than 0.5 mm is negligible. For a computational fluid dynamics simulation in a complex two- or three-dimensional intestinal space, solving the diffusion equation for evolving food particles in a long digestion process would demand computational resources far beyond current capabilities (Ho et al., 2013). This finding provides effective evidence supporting the need for model simplification in future work.

3.4. Significance of species transport in the intestine

The transport function of the intestinal tract gives rise to the change in the spatial distribution of particles and pancreatic enzyme. However, traditional *in-vitro* digestion experiments, widely employed for assessing the digestion kinetics of various foods, are typically homogeneous systems. In order to analyze the effect of intestinal transport, this section constructs a contrast model representing a homogeneous system where both enzyme and particles are instantly dispersed throughout the entire intestine after being emptied from the stomach. The mass conservation equation Eq. (1) is modified to different forms for enzyme, maltose and glucose, respectively:

$$\frac{\partial C_{l,e}}{\partial t} = \frac{J_e}{\pi {R_i}^2 L} \tag{36}$$

$$\frac{\partial C_{l,m}}{\partial t} = \frac{\int_0^L G_{sm} dz}{L} \tag{37}$$

$$\frac{\partial C_{l,g}}{\partial t} = \frac{\int_0^L G_{mg} dz}{L} \tag{38}$$

Similarly, revising Eq. (2) for particle distribution gives:

$$\frac{\partial n_p}{\partial t} = \frac{\gamma n_{sto}}{\pi {R_i}^2 L} \tag{39}$$

A group of spherical rice particles of 0.5 mm initial size was investigated. Fig. 9(a) displays the results obtained by the original model (solid line) and the contrast model (dashed line). The absence of transport phenomenon in the intestine decreases the digestion ratio by 13 % and the absorption ratio by 14 % at 1 h. The underestimation of digestion behavior consequently results in a 16.3 % reduction in the peak blood glucose level. The discrepancy arises from the attenuation of enzyme concentration in a homogeneous system. As depicted in Fig. 9 (b), the average concentration of the enzyme on the particle surface computed by the contrast model is markedly lower, though gradually growing as a result of the continuous intestinal secretion of enzyme. By comparison, the established model considering intestinal transport achieves a substantially higher level, approaching the range (150 ~ 300 U/ml) summarized by Keller and Layer (2005) from prior human experiments. All the enzyme concentrates in regions containing particles rather than dispersing over the whole tube. Undoubtably, it leads to higher concentration difference between the exterior and interior of pores particles, facilitating the inward diffusion of the enzyme.

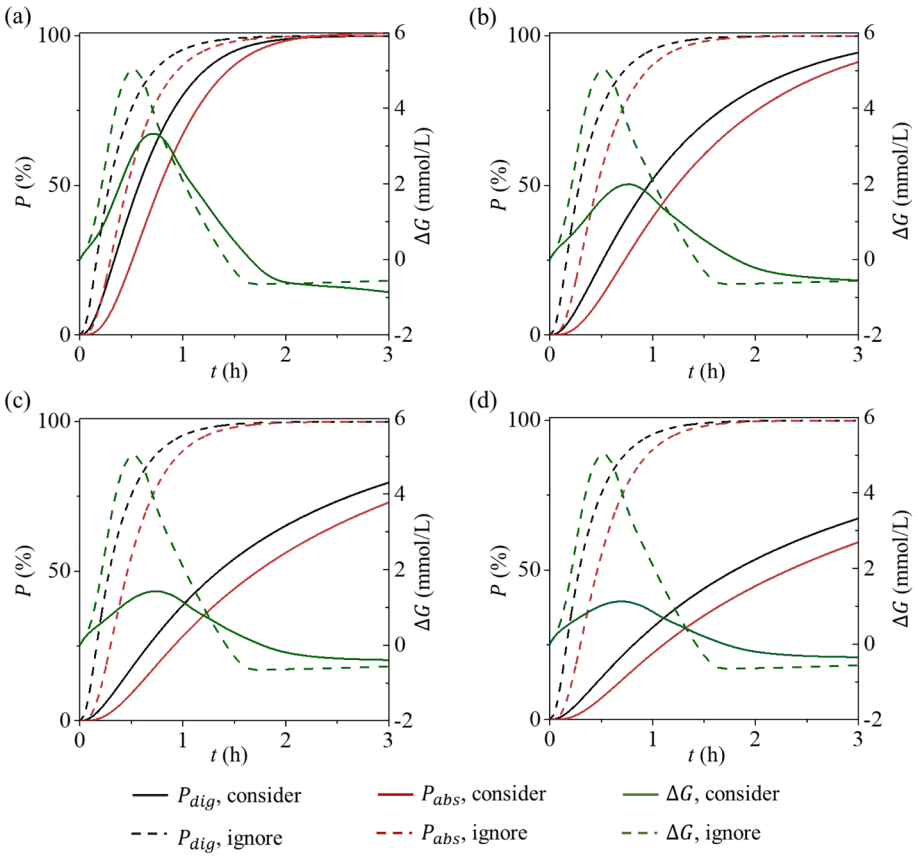

Fig. 8. Simulation results of starch digestion, glucose absorption and glycemic change when considering or ignoring granular diffusion resistance for different initial particle sizes (a) 0.5 mm (b) 1 mm (c) 1.5 mm (d) 2 mm.

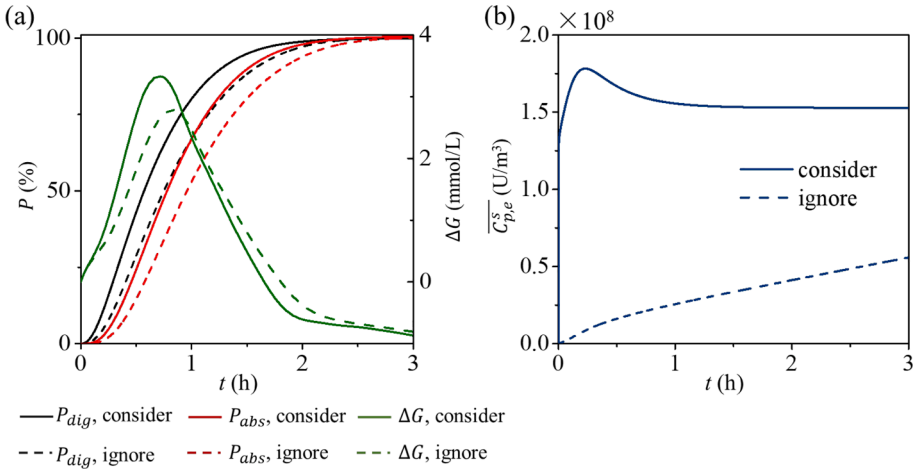

Fig. 9. Simulation results when considering or ignoring species transport in the intestine. (a) starch digestion, glucose absorption and glycemic change (b) average enzyme concentration on the surface of particles.

4. Conclusion

This work proposed a multiscale model for characterizing the digestion behavior of starch particles in the intestine. By incorporating other glycemic-related processes, a dietary property-based glycemic prediction system has been developed. Sample calculations referring to previous human experiments verified the model effectiveness. The effect of initial particle size on digestion has been fully captured. The model-based analysis gives insights into the granular evolutions in terms of intrinsic properties and solute concentration, which is difficult to obtain by experimental approaches. Moreover, this study highlights that both particle-scale diffusion resistance and intestine-scale transport phenomenon are very critical for the prediction of *in-vivo* starch-based food digestion. Within the particle size range researched herein, ignoring the former mechanism underrates the glycemic peak by at least half. Regarding cereal granules with fewer pores and channels, the diffusion resistance within the particle is expected to be more remarkable.

The current modeling approach, however, has its disadvantages, as it is challenging to describe the effects of diverse complex intestinal features, such as curved geometry and wall motility. We are now

developing a multi-physics model that can characterize these complex features in 3D space and explore their effects on the digestion of starch particles. All these efforts are expected to improve the predictive accuracy of *in-vivo* food digestion and postprandial glycemic response.

CRediT authorship contribution statement

Yifan Qin: Writing – original draft, Validation, Software, Methodology, Investigation, Formal analysis, Data curation, Conceptualization. **Jie Xiao:** Writing – review & editing, Supervision, Software, Methodology, Conceptualization. **Aibing Yu:** Supervision, Funding acquisition, Conceptualization. **Xiao Dong Chen:** Writing – review & editing, Supervision, Project administration, Funding acquisition, Conceptualization.

Declaration of competing interest

The authors declare that they have no known competing financial interests or personal relationships that could have appeared to influence the work reported in this paper.

Data availability

Data will be made available on request.

Acknowledgments

The authors are grateful for the financial support from the National Natural Science Foundation of China (22078212 & 21978184). Thanks also go to Particle Engineering Laboratory (China Petroleum and Chemical Industry Federation) at Soochow University. Prof. Jie Xiao acknowledges the “Jiangsu Innovation and Entrepreneurship (Shuang Chuang) Program” and the “Jiangsu Specially-Appointed Professors Program”.

Appendix A

The equations identical to those in the original version (Qin et al., 2023(b)) are provided below. The description of symbols is given in Nomenclature.

$$D_{p,x} = \frac{k_B T \varepsilon}{3\pi\mu d_x \tau} F_1(\varphi) F_2(\varphi) \tag{A1}$$

$$\varphi_x = \frac{d_x}{d_{pore}} \tag{A2}$$

$$d_{pore} = d_{pore,0}\sqrt{\frac{\varepsilon}{\varepsilon_0}} \tag{A3}$$

$$F_{1,x} = (1-\varphi_x)^2 \tag{A4}$$

$$F_{2,x} = 1 - 2.104\varphi_x + 2.09{\varphi_x}^3 - 0.95{\varphi_x}^5 \tag{A5}$$

$$\varepsilon = 1 - (1-\varepsilon_0)\frac{X}{X_0} \tag{A6}$$

$$\eta = \eta_0 \frac{X_0}{X} \tag{A7}$$

$$A_i = A_{i,0}\sqrt{\frac{\varepsilon}{\varepsilon_0}} \tag{A8}$$

$$X = X_{dig} + X_{indig} \tag{A9}$$

$$X_{indig} = X_{indig,0} \tag{A10}$$

Appendix B

According to the discretization scheme stated in the numerical method, Eq. (1) becomes:

$$C_{l,x}^{i,j+1} = C_{l,x}^{i,j} - \frac{\Delta t \overline{u}}{\Delta z}\left(C_{l,x}^{i,j} - C_{l,x}^{i-1,j}\right) + S_{l,x}^{i,j}\Delta t \tag{B1}$$

and Eq. (32) becomes:

$$\begin{aligned} C_{p,x}^{k,i+1,j+1} = {} & \left[1 - \frac{2D_{p,x}^{k,i,j}\Delta t}{\left(R_p^{k,i,j}\right)^2 \left(\Delta r^*\right)^2}\right] C_{p,x}^{k,i,j} + \left[\frac{r^*\left(R_p^{k,i+1,j+1} - R_p^{k,i,j}\right)}{2R_p^{k,i,j}\Delta r^* \Delta t} + \frac{D_{p,x}^{k+1,i,j} - D_{p,x}^{k-1,i,j} + 4D_{p,x}^{k,i,j}}{4R_{k,i,j}^2\left(\Delta r^*\right)^2} + \frac{(\lambda-1)D_{p,x}^{k,i,j}}{2R_{k,i,j}^2 r^* \Delta r^*}\right] C_{p,x}^{k+1,i,j}\Delta t \\ & + \left[\frac{D_{p,x}^{k-1,i,j} - D_{p,x}^{k+1,i,j} + 4D_{p,x}^{k,i,j}}{4R_{k,i,j}^2\left(\Delta r^*\right)^2} - \frac{r^*\left(R_p^{k,i+1,j+1} - R_p^{k,i,j}\right)}{2R_{k,i,j}\Delta r^* \Delta t} - \frac{(\lambda-1)D_{p,x}^{k,i,j}}{2R_{k,i,j}^2 r^* \Delta r^*}\right] C_{p,x}^{k-1,i,j}\Delta t + S_{p,x}^{k,i,j}\Delta t \end{aligned} \tag{B2}$$

References

Bajaj, R., Singh, N., Kaur, A., & Inouchi, N. (2018). Structural, morphological, functional and digestibility properties of starches from cereals, tubers and legumes: A comparative study. *Journal of Food Science and Technology, 55*(9), 3799–3808.

Czakó, L., Hajnal, F., Németh, J., Tákács, T., & Lonovics, J. (1999). Effect of a liquid meal given as a bolus into the jejunum on human pancreatic secretion. *Pancreas, 18*(2), 197–202.

Dahlqvist, A., & Thomson, D. L. (1963). The digestion and absorption of maltose and trehalose by the intact rat. *Acta Physiologica Scandinavica, 59*, 111–125.

Dalla Man, C., Camilleri, M., & Cobelli, C. (2006). A system model of oral glucose absorption: Validation on gold standard data. *IEEE Transactions on Biomedical Engineering, 53*(12), 2472–2478.

Dalla Man, C., Rizza, R. A., & Cobelli, C. (2007). Meal simulation model of the glucose-insulin system. *IEEE Transactions on Biomedical Engineering, 54*(10), 1740–1749.

Dhital, S., Warren, F. J., Butterworth, P. J., Ellis, P. R., & Gidley, M. J. (2017). Mechanisms of starch digestion by α-amylase—Structural basis for kinetic properties. *Critical Reviews in Food Science and Nutrition, 57*(5), 875–892.

Ellis, P., Roberts, F., Low, A., & Morgan, L. (1995). The effect of high-molecular-weight guar gum on net apparent glucose absorption and net apparent insulin and gastric inhibitory polypeptide production in the growing pig: Relationship to rheological changes in jejunal digesta. *British Journal of Nutrition, 74*(4), 539–556.

Fatima, J., Iqbal, C. W., Houghton, S. G., Kasparek, M. S., Duenes, J. A., Zheng, Y., & Sarr, M. G. (2009). Hexose transporter expression and function in mouse small intestine: Role of diurnal rhythm. *Journal of Gastrointestinal Surgery, 13*, 634–641.

Goñi, I., Garcia-Alonso, A., & Saura-Calixto, F. (1997). A starch hydrolysis procedure to estimate glycemic index. *Nutrition Research, 17*(3), 427–437.

Gres, S., & Jeffrey, G. (1977). A neutron diffraction refinement of the crystal structure of β-maltose monohydrate. *Acta Crystallographica Section B: Structural Crystallography and Crystal Chemistry, 33*(8), 2490–2495.

Guyton, A., & Hall, J. (2006). *Textbook of medical physiology, 11th*. Philadelphia: Elsevier Inc.

Ho, Q. T., Carmeliet, J., Datta, A. K., Defraeye, T., Delele, M. A., Herremans, E., Opara, L., Ramon, H., Tijskens, E., van der Sman, R., Liedekerke, P. V., Verboven, P., & Nicolaï, B. M. (2013). Multiscale modeling in food engineering. *Journal of Food Engineering, 114*(3), 279–291.

Illingworth, T. C., & Golosnoy, I. O. (2005). Numerical solutions of diffusion-controlled moving boundary problems which conserve solute. *Journal of Computational Physics, 209*, 207–225.

Keller, J., & Layer, P. (2005). Human pancreatic exocrine response to nutrients in health and disease. *Gut, 54*, 1–28.

Lennernäs, H., Palm, K., Fagerholm, U., & Artursson, P. (1996). Comparison between active and passive drug transport in human intestinal epithelial (Caco-2) cells in vitro and human jejunum in vivo. *International journal of pharmaceutics, 127*(1), 103–107.

Lentle, R. G., & Janssen, P. W. (2011). *The physical processes of digestion*. New York: Springer Science & Business Media.

Mackie, A. R., Bajka, B. H., Rigby, N. M., Wilde, P. J., Alves-Pereira, F., Mosleth, E. F., Rieder, A., Kirkhus, B., & Salt, L. J. (2017). Oatmeal particle size alters glycemic index but not as a function of gastric emptying rate. *American Journal of Physiology-Gastrointestinal and Liver. Physiology, 313*(3), G239–G246.

Moxon, T. E., Gouseti, O., & Bakalis, S. (2016). In silico modelling of mass transfer & absorption in the human gut. *Journal of food engineering, 176*, 110–120.

Moxon, T. E., Nimmegeers, P., Telen, D., Fryer, P. J., Van Impe, J., & Bakalis, S. (2017). Effect of chyme viscosity and nutrient feedback mechanism on gastric emptying. *Chemical Engineering Science, 171*, 318–330.

Nadia, J., Bronlund, J., Singh, R. P., Singh, H., & Bornhorst, G. M. (2021). Structural breakdown of starch-based foods during gastric digestion and its link to glycemic response: In vivo and in vitro considerations. *Comprehensive Reviews in Food Science and Food Safety, 20*(3), 2660–2698.

Nilsson, A., Granfeldt, Y., Ostman, E., Preston, T., & Bjorck, I. (2006). Effects of GI and content of indigestible carbohydrates of cereal-based evening meals on glucose tolerance at a subsequent standardised breakfast. *European Journal of Clinical Nutrition, 60*(9), 1092–1099.

Oviedo, S., Vehi, J., Calm, R., & Armengol, J. (2017). A review of personalized blood glucose prediction strategies for T1DM patients. *International journal for numerical methods in biomedical engineering, 33*(6), e2833.

Park, H. M. (2018). A multiscale modeling of fixed bed catalytic reactors. *International Journal of Heat and Mass Transfer, 116*, 520–531.

Payan, F., Haser, R., Pierrot, M., Frey, M., Astier, J., Abadie, B., Duée, B., & Buisson, G. (1980). The three-dimensional structure of α-amylase from porcine pancreas at 5 Å resolution–the active-site location. *Acta Crystallographica Section B: Structural Crystallography and Crystal Chemistry, 36*(2), 416–421.

Qin, Y., Chen, X. D., Yu, A., & Xiao, J. (2023a). New understanding from intestinal absorption model: How physiological features influence mass transfer and absorption. *AIChE Journal, 69*(8), e18099.

Qin, Y., Xiao, J., Yu, A., & Chen, X. D. (2023b). A starch digestion model considering intrinsic granular properties. *Journal of Food Engineering, 369*, Article 111918.

Ranawana, V., Monro, J. A., Mishra, S., & Henry, C. J. K. (2010). Degree of particle size breakdown during mastication may be a possible cause of interindividual glycemic variability. *Nutrition research, 30*(4), 246–254.

Ranawana, V., Clegg, M. E., Shafat, A., & Henry, C. J. (2011). Postmastication digestion factors influence glycemic variability in humans. *Nutrition Research, 31*(6), 452–459.

Tortora, G. J., & Derrickson, B. H. (2018). *Principles of anatomy and physiology* (14th edition). New York: John Wiley & Sons Inc.

van Boekel, M. A. (2008). *Kinetic modeling of reactions in foods*. New York: CRC Press.

Zhou, Z., Topping, D. L., Morell, M. K., & Bird, A. R. (2010). Changes in starch physical characteristics following digestion of foods in the human small intestine. *British Journal of Nutrition, 104*(4), 573–581.